signal emanating from the apical ectoderm. As *in situ* hybridization does not detect very low amounts of transcripts, it is unclear whether the activation of these genes represents stimulation or *de novo* expression. The characteristic amounts of activity and regions of expression of *Hox-7.1* and *Hox-8.1* may be specified by different threshold responses to the signal. One candidate is BMP-2A, a member of the transforming growth-factor family, which is expressed in the ventral ectoderm of the early mouse limb and later confined to the apical ridge[8].

The rapid activation of *Hox-7.1* and *Hox-8.1* in tissue placed in the progress zone is consistent with a primary function for these genes in limb-pattern formation. Many other genes are expressed in the limb bud that may act with, or be regulated by, *Hox-7.1* and *Hox-8.1*. These include several homeobox-containing genes[9] and others that are likely to have morphogenetic functions, retinoic acid receptors and binding protein[10,11], int-related[12] and AP-2 (ref. 13). In contrast to *Hox-7.1* and *Hox-8.1*, at least some of these genes seem not to be rapidly responsive to positional cues. The activity of a chick gene homologous to the *XlHbox1* gene of *Xenopus* appears to be cell autonomous in reciprocal anteroposterior grafts in limbs[14]. In addition, new transcripts of chick genes homologous to genes of the mouse HOX-4 complex, which are induced in distal mesoderm of chick wing buds that will give a duplicated pattern, only reach detectable levels after 16–24 h suggesting an indirect response to positional signals[15].

To test critically the hypothesis that *Hox-7.1* and *Hox-8.1* play a part in proximodistal pattern formation in the limb, it will be necessary to examine the effects of changes in gene expression on limb development. The ability to regulate *Hox-7.1* and *Hox-8.1* in tissue grafted to the limb provides an assay which may be useful in identifying the signals and responsive elements that control their developmental expression. Ultimately manipulation of these controls may provide a means to examine the roles of *Hox-7.1* and *Hox-8.1* in the development of the limb skeleton. □

Received 20 February; accepted 7 June 1991.

1. Ingham, P. W. *Nature* **335,** 25–34 (1988).
2. Wolpert, L., Lewis, J. & Summerbell, D. in *Cell Patterning* CIBA Symposium (new series) 95–119 (Associated Scientific, Amsterdam, 1975).
3. Hill, R. E. *et al. Genes Dev.* **3,** 26–37 (1989).
4. Robert, B., Sassoon, D., Jacq, B., Gehring, W. & Buckingham M. EMBO J. **8,** 91–100 (1989).
5. Summerbell, D., Lewis, J. & Wolpert, L. *Nature* **244,** 492–496 (1973).
6. Saunders, J. W., Gasseling, M. W. & Cairns, J. M. *Devl Biol.* **1,** 281–301 (1959).
7. Cairns, J. M. *Devl Biol.* **12,** 36–52 (1965).
8. Lyons, K. M., Pelton, R. W. & Hogan, B. L. M. *Development* **109,** 833–844 (1990).
9. Dollé, P., Izpisúa-Belmonte, J.-C., Falkenstein, H., Renucci, A. & Duboule, D. *Nature* **342,** 767–772 (1989).
10. Dollé, P. *et al. Nature* **342,** 702–704 (1989).
11. Dollé, P., Ruberte, E., Leroy, P., Morriss-Kay, G. & Chambon, P. *Development* **110,** 1133–1151 (1990).
12. Gavin, B. J., McMahon, J. A. & McMahon, A. P. *Genes Dev.* **4,** 2319–2332 (1990).
13. Mitchell, P., Timmons, P. M., Herbert, J. M., Rigby, P. W. J. & Tjian, R. *Genes Dev.* **5,** 105–119 (1991).
14. Oliver, G., De Robertis, E. M., Wolpert, L. & Tickle, C. *EMBO J.* **9,** 3093–3101 (1990).
15. Izpisúa-Belmonte, J.-C., Tickle, C., Dollé, P., Wolpert, L. & Duboule, D. *Nature* **350,** 585–589.
16. Davidson, D. R., Graham, E., Sime, C. & Hill, R. E. *Development* **104,** 305–316 (1988).
17. Jorquera, B. & Pugin, E. *C.r. hebd. Séanc. Acad. Sci., Paris* **272,** 1522–1525 (1971).
18. Tickle, C., Shellswell, G., Crawley, A. & Wolpert, L. *Nature* **259,** 396–397 (1976).
19. Hamburger, V. & Hamilton, H. L. *J. Morphol.* **50,** 217–233 (1979).
20. Cottrill, C., Crawley, A. & Tickle, C. *Cell Differ. Dev.* **29,** 67–80 (1990).

ACKNOWLEDGEMENTS. We thank L. Wolpert and H. J. Evans for helpful suggestions. C.T. was supported by The Royal Society.

Sodium channel density in hypomyelinated brain increased by myelin basic protein gene deletion

J. L. Noebels, P. K. Marcom & M. H. Jalilian-Tehrani*

Developmental Neurogenetics Laboratory, Section of Neurophysiology, Department of Neurology, Division of Neuroscience, Institute of Molecular Genetics, and * Department of Biochemistry, Baylor College of Medicine, Houston, Texas 77030, USA

TROPHIC control over the expression and membrane distribution of voltage-dependent ion channels is one of the principal organizing events underlying the maturation of excitable cells. The myelin sheath is a major structural determinant of regional ion channel topography in central axons[1,2], but the exact molecular signals that mediate local interactions between the oligodendrocyte and axolemma are not known. We have found that large caliber fibre pathways in the brain of the mutant mouse *shiverer* (*shi*, gene on chromosome 18), whose developmental fate of myelination is averted by deletion of five exons in the myelin basic protein gene[3–5], have a striking excess of sodium channels. As cytoplasmic membranes of *shiverer* oligodendroglia still adhere to axons[6–8], the evidence indicates that myelin basic protein or a myelin basic protein-dependent glial transmembrane signal associated with compact myelin formation, rather than a simple glial–axon contact inhibition or an intrinsic genetic program of neuronal differentiation, could be critical in downregulating sodium channel density in axons. Here we use the *shiverer* mutant to show that mature central nervous system projection neurons with large caliber unmyelinated fibres sustain functional excitability by increasing sodium channel density. This axon plasticity, triggered by the absence of a single glial protein, contributes to the unexpectedly mild degree of neurological impairment in the mutant brain without myelin, and may be a potentially inducible mechanism determining the recovery of function from dysmyelinating disease.

We prepared autoradiograms of adult *shi/shi* and +/+ brain sections and performed regional binding assays with tritiated saxitoxin, which binds externally to the membrane-bound[9] but not to the free intracellular form[10] of the sodium channel α subunit, the peptide requisite for ion conduction[11]. Autoradiography revealed striking increases (2.2–4.7-fold) in silver grain density, reflecting specific ^{3}H-saxitoxin binding over all hypomyelinated *shiverer* fibre tracts when compared with +/+ brains (Fig. 1). Within mixed grey matter regions the increases are less striking (1.1–1.4-fold) and reflect the proportional content of hypomyelinated fibres of passage (Table 1). In the most homogeneous nuclear regions, where only a small fractional area consists of penetrating hypomyelinated fibres, there is little difference between genotypes. One such region, the outer molecular layer of cerebellar cortex, comprises an essentially pure population of unmyelinated parallel fibres showing one of the highest sodium channel densities in the brain; binding in this layer is unaltered by the mutant gene, indicating that the channel density increase is nonuniform and predominates in hypomyelinated axon pathways.

To determine whether the density increase in the mutant was due to an alteration in the number of receptors, their affinity, or both, we performed specific binding experiments on freshly dissected central nervous system (CNS) homogenates solubilized in excess scintillant in which lipid quenching is essentially zero. Samples composed of hypomyelinated fibres (optic nerve), mixed cellular neuropil (neocortex) and whole brain were used for saturation studies. Specific binding was saturable in both genotypes. Scatchard analysis showed the presence of a single binding site, and toxin affinity was not significantly different between genotypes (Fig. 2). In contrast, the number of binding sites (B_{max}) in mutants was 3–4-fold higher in optic nerve and 1.6-fold higher in neocortex than it was in control mice. The level of specific toxin binding in heterogeneous brain areas was 10–35% higher in the mutant than in corresponding control regions (Table 2).

The ^{3}H-saxitoxin density increase in hypomyelinated pathways may not be confined to axons, and we do not exclude the possible addition of sodium channels at adjacent non-neuronal sites. Oligodendroglia do not express sodium channels[12], but astroglia show ^{3}H-saxitoxin binding and voltage-dependent sodium currents[13] and are relatively increased in *shiverer* pathways[3,6,8]. Although astrocytes may contribute a fraction of the ^{3}H-saxitoxin binding increase in hypomyelinated brain, two lines of evidence favour an axonal origin. First, instead of flaccid or spastic paralysis, the *shiverer* mutant shows an unexpected neurological phenotype of normal motor strength and tone, consistent with intact impulse conduction in corticospinal pathways. Astroglial sodium channels cannot account for persistent conduction across inexcitable internodal membrane by any known mechanism. Second, an increase in axolemmal sodium channels would predict associated elevations in axonal (Na^++ K^+)ATPase and cytochrome oxidase activity to fuel the metabolic demand of restoring ionic gradients; both have been identified in *shiverer* pathways[14] (J.L.N., unpublished results). We conclude that a substantial fraction of the ^{3}H-saxitoxin density increase is localized on central axons.

Although intermediate stages of axolemmal sodium channel arrangement during myelinogenesis have not been fully clarified in mammalian CNS axons, glia are important determinants of the final topography. Ultrastructural observations of external face intramembraneous particle distributions indicate that where myelin does not form, the axolemma fails to differentiate, and that where myelin forms abnormally, there are corresponding abnormalities in the axolemma[1,2,15]. As sodium ion-mediated impulse conduction precedes myelination in developing CNS pathways[16,17], and few if any sodium channels are found along the acutely desheathed adult internode[18], acquisition of myelin must be accompanied by a controlled reduction and rearrangement of the native distribution of axolemmal sodium channels in the recipient neuron. There are two major hypotheses on the cellular origin of signals regulating this rearrangement. The neuronal hypothesis, based on indirect evidence that intramembraneous particle clusters form in the absence of myelinating cells[15], specifies that some degree of specialized nodal–internodal architecture arises from constitutive gene expression in the differentiating neuron. The glial hypothesis, supported in part by inhibitory responses of axons to specific oligodendroglial molecules[19], stipulates a secondary suppression of internodal channels after contact with the myelinating cell. If sodium channel arrangement in axons were regulated solely by the parent neuron according to the first hypothesis, ^{3}H-saxitoxin binding in myelin-deprived fibres would not differ from control fibres. This prediction is contradicted by our results, which favour a mechanism of axon channel remodelling directed by glia, wherein the developing neuron maintains an ion channel density optimal for its caliber[20] until an inhibitory glial signal is received.

TABLE 1 Gene-linked alterations in specific ^{3}H-saxitoxin binding to *shiverer* and +/+ brain regions (fmol mg^{-1} protein)

Region	+/+	*shi/shi*	Per cent of control
Myelinated tracts:			
Optic nerve	5.8 ± 6.6	27.2 ± 11.1	468.9*
Corpus callosum	77.7 ± 63.6	178.6 ± 55.4	229.9*
Anterior commissure	58.8 ± 55.8	176.2 ± 21	299.6*
Fimbria	54.6 ± 28.6	161.7 ± 40.9	296.2*
Alveus	72.1 ± 34.9	233.8 ± 59.2	324.3*
Internal capsule	67.2 ± 31	43.8 ± 34.1	214.0*
Fornix	52.1 ± 34.5	114.4 ± 39.3	219.5†
Unmyelinated:			
Cerebellar molecular layer	340.8 ± 37.3	351.5 ± 43.5	103.1 (NS)
Predominantly nuclear:			
Neocortex	138.1 ± 22.5	193.9 ± 31.5	140.4*
Substantia Nigra	196.5 ± 41.7	248.4 ± 37.8	126.4*
Periaquaductal grey	132.6 ± 33	184.7 ± 32	142.9*
Cerebellar granule cell	89.3 ± 24.2	121.8 ± 38.4	136.4*
Thalamus	118.3 ± 47.1	151.1 ± 44.9	127.7†
Hippocampus	139.8 ± 41.7	155.7 ± 36.2	111.4 (NS)
Septum	141.0 ± 62.2	159.4 ± 61.5	113.1 (NS)
Hypothalamus	150.8 ± 64	170.4 ± 42.4	119.0 (NS)
Sup. Colliculus	175.6 ± 51	232.0 ± 43.8	134.0 (NS)
Mixed fibre/nuclear			
Anterior midbrain	58.7 ± 24.3	161.0 ± 27	274.3*
Pons	67.6 ± 31.7	162.5 ± 38.5	282.1*
Cerebellum	162.7 ± 23	197.8 ± 30.8	121.6*
Striatum	96.6 ± 48	137.9 ± 48	142.7*
Midbrain	83.7 ± 24	169.7 ± 27.1	202.8*
Whole brain sections	129.2 ± 39.7	175.2 ± 37.5	135.6*

Integrated optical densitometry was used to quantitate silver grain densities. The analog video signal was corrected for background illumination and digitized (Loates) so that the optical density of each 3 × 3 micron area of the film, corresponding to one pixel, represented a value from 0–225. The absolute value for tissue densities of ^{3}H-saxitoxin was determined using a calibration curve derived from standards exposed on the same film. Specific binding was determined by subtracting nonspecific from total binding using optical overlays. Densities were sampled from 30 brain regions at 8 ascending levels of the neuraxis in 3 mice of each genotype by taking the mean of triplicate square 'punches' within the perimeter. Boundaries of heterogenous regions were circumscribed and measured as a unit. Specific binding in each region was averaged across all samples and compared by genotype using the Student's two-tailed *t*-test. Quantitative autoradiography with tritiated ligands is corrected for differential β emission absorption by lipids because tritium efficiency is lower over myelinated regions[28]. Although *shiverer* oligodendrocytes are not numerically reduced[3], the secondary wrappings only loosely envelop axons, and total lipid levels are ~20–30% lower in the mutant's CNS (ref. 29). When the calculated densities are corrected using a maximal quench correction factor of 0.3, specific ^{3}H-saxitoxin binding within hypomyelinated *shiverer* fibre tracts remains significantly high compared with +/+ pathways. Two geometric factors, a potential reduction in either fibre diameter or interaxonal spacing within the pathway, do not apparently account for the density increase. Mean axon circumferences were reduced by <6% in a sample of 1,800 *shi/shi* (2.25 μm) and +/+ (2.39 μm) optic nerve axons (H. D. Shine, personal communication), and white matter tract widths in Luxol Fast blue stained sections were directly superimposable, suggesting that fibre diameter and packing density are little affected by the loose glial wrapping.

* $P < 0.001$; † $P < 0.05$; NS, not significant.

TABLE 2 Specific binding of ^{3}H-saxitoxin to +/+ and *shi/shi* brain regions *in vitro*

Tissue	Specific binding (fmol mg^{-1}) +/+	*shi/shi*	Per cent of control
Neocortex (n = 5)	285.9 ± 12.9	385.5 ± 36.8	135*
Hippocampus (n = 3)	464.3 ± 5.1	512.73 ± 3	110*
Cerebellum (n = 5)	466.9 ± 21.4	547.0 ± 7.9	117†
Whole brain (n = 4)	369.8 ± 19.7	469.7 ± 32.3	127‡

Means ± s.e. of the number of experiments in parentheses (each in triplicate determinations). Dissected brain regions were homogenized in incubation buffer (20 mM Tris–HCl, pH 7.4, containing 140 mM *N*-methyl glucamine, 5.4 mM KCl, 2.8 mM $CaCl_2$ and 1.3 mM $MgSO_4$) at 4 °C. In preliminary experiments toxin binding at 4 °C was complete at 45 min using constant radioligand concentrations of 5 nM. Specific binding accounted for ~90% of total binding. Specific binding of ^{3}H-saxitoxin in the presence of increasing concentrations of cellular protein was linear up to 350 μg and freezing did not reduce the linearity or extent of binding. For saturation studies, aliquots of 120–200 μg cellular protein were added to an assay mixture containing 5 nM ^{3}H-saxitoxin in a final volume of 100 μl. Assays used to define nonspecific binding also contained 1 μM tetrodotoxin. The mixture was incubated for 60 min at 4 °C, terminated by addition of 3.5 ml ice-cold buffer and filtered through GF/C filters. Filters were washed twice with buffer, dried, and the radioactivity assayed by liquid scintillation counting.

* $P < 0.025$; † $P < 0.001$; ‡ $P < 0.05$.

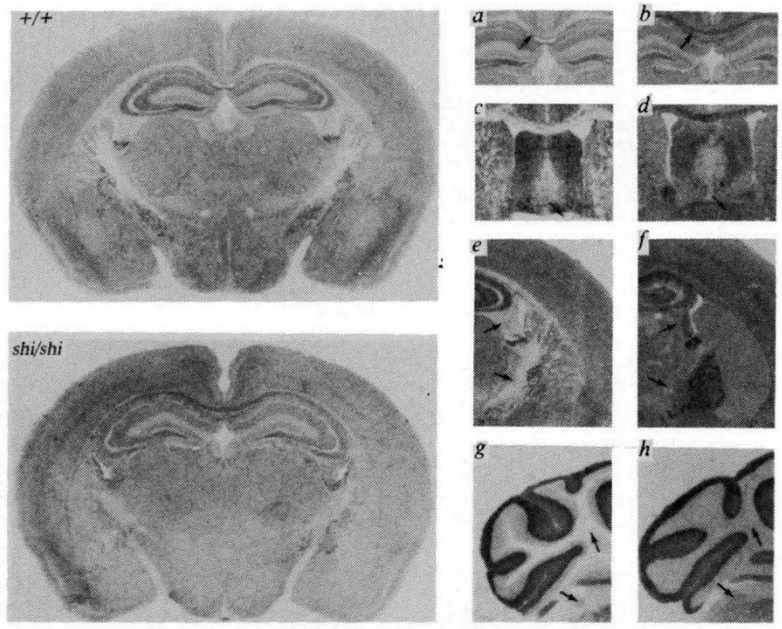

FIG. 1 Left: Autoradiograms of specific ^{3}H-saxitoxin binding in adult wild-type and *shiverer* mouse brain reveal increases in sodium channel density within hypomyelinated mutant central axon tracts. Right: Regional ^{3}H-saxitoxin binding in +/+ (*a, c, e, g*) compared with *shi/shi* (*b, d, f, h*) pathways is indicated by arrows: *a–b*, corpus callosum; *c–d*, anterior commissure; *e–f*, hippocampal fimbria (upper arrow) and internal capsule (lower); *g–h*, cerebellar white matter (upper) and inferior cerebellar peduncle (lower).

METHODS. ^{3}H-saxitoxin autoradiography: Coronal cryostat sections (20 microns) were cut from fresh adult (3–4 months postnatal) homozygous male *shi/shi* (C57Bl/6-shi) and C57Bl/6 (+/+) brains at 8 predesignated levels of the neuraxis rostral to the medulla. Fozen sections were thaw-mounted on gel alumin-subbed slides and dried in a dessicator overnight at 4 °C. Slides from each genotype were matched into sets for binding using adjacent cresyl violet-stained sections to verify comparable neuroanatomical planes of section. Matched slides were simultaneously incubated with 5 nM ^{3}H-saxitoxin (Amersham) at 4 °C for 60 min in incubation buffer (20 mM Tris–HCl, pH 7.4, containing 140 mM *N*-methyl glucamine, 5.4 mM KCl, 2.8 mM $CaCl_2$ and 1.3 mM $MgSO_4$) according to Mourre *et al.*[30]. Incubation was terminated by 2×5-second washes in ice-cold buffer and a quick rinse in distilled water, then sections were dried under cold air. Non-specific binding was determined in adjacent sections by preincubation with 1 μM tetrodotoxin (Sigma). Slide pairs of specific and nonspecific binding from the two genotypes were then placed side-by-side on the same sheet of Hyperfilm ^{3}H with glass-mounted ^{3}H calibration standards (Microscale, Amersham), exposed in cassettes for 2–3 weeks and developed in the same way.

Shiverer axons present two important clues regarding the nature of this signal and the source of the channels. Although close apposition of glial plasma membranes could present a steric barrier to the free lateral movement of axolemmal cation-selective channel proteins with large external domains (~60 nm) in +/+ fibres, it is unlikely that a lack of simple physical contact alone could mediate the increase in sodium channel density in the mutant. Despite the absence of multilammellar compact myelin in *shiverer*, the primary oligodendroglial membrane wrapping adheres to the internodal axolemma at irregularly spaced axoglial junctions with the usual ~20–30 nm gap; these appositions are even more prevalent in mutant than in wild-type axons[7]. Furthermore, because the absolute number of sodium channels in *shiverer* hypomyelinated pathways is raised, impulse conduction is less likely to be preserved by spatial redistribution of existing nodal channels than by increased stabilization of new channels in the bilayer. Our data therefore suggest that the immediate presence of one or more of the six myelin basic protein isoforms expressed in normal mouse CNS myelin[21,22] or of other related myelin components whose expression may be linked to that of MBP (for example, proteolipid protein[23] and myelin-associated glycoprotein[14,24]), but not glial–axonal membrane adhesion alone, is a prime signal regulating sodium channel density in adult axons.

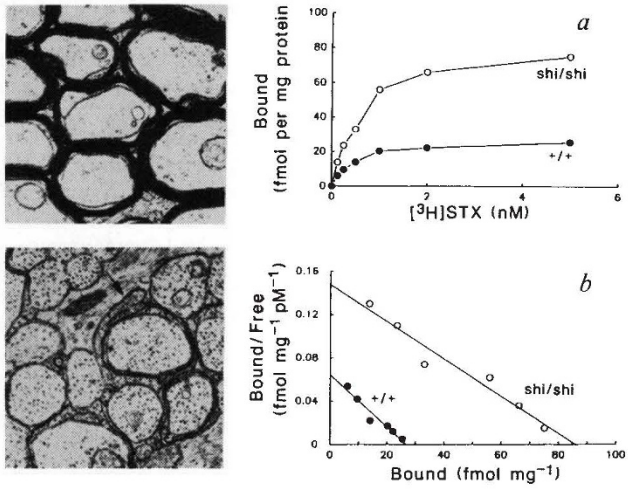

FIG. 2 Left: Ultrastructure of myelinated +/+ (upper) and hypomyelinated *shi/shi* fibres without myelin basic protein (lower) in adult optic nerve shows glial adhesion and absence of compact myelin with loose oligodendrocyte wrappings in mutant axons (arrow). Right: *a*, Representative data from one experiment showing dose-dependent specific binding of ^{3}H-saxitoxin (STX) to optic nerve axons from +/+ and *shi/shi* mice (method described in legend to Table 2). In each experiment optic nerve samples from *shi/shi* (n=20) and +/+ (n=12) mice were pooled to obtain adequate protein specimens for triplicate binding assays. *b*, Scatchard analysis of data in *a* gave K_d=0.42; B_{max}=27.6±2 (+/+) and K_d=0.58; B_{max}=85.8±8 (*shi/shi*). Repeat assays produced similar values. Identical experiment using neocortex produced values for K_d=0.29; B_{max}=227.1±10 (+/+) and K_d=0.28; B_{max}=376.5±21 (*shi/shi*).

Acute neurological deficits that accompany the demyelinating lesions of multiple sclerosis in human white matter confirm estimates predicting impulse conduction failure at inexcitable regions exposed by the injured oligodendrocyte, but clinical remission without total fibre remyelination[25] and signs of ectopic axon hyperexcitability[26] (both consistent with increased sodium channel density[20]) are frequently found in patients recovering from this disease. The evidence for functional axon conduction with increased sodium channel density in the hypomyelinated brain lacking myelin basic protein suggests that demyelinated CNS fibres in multiple sclerosis may regain excitability by a similar mechanism once the inhibitory influence of a myelin membrane protein is removed. The *shiverer* mutation identifies myelin basic protein as a candidate glial suppressor protein involved in the trophic regulation of neuronal sodium channels. Further elucidation of the entire signalling sequence linking glial membrane proteins to the regulation of sodium channel α-subunit gene transcription[27] may suggest specific strategies for the clinical management of ion channel gene expression in dysmyelinating disease. □

Received 3 April; accepted 18 June 1991.

1. Waxman, S. G. *Prog. Brain Res.* **71,** 121–141 (1987).
2. Rosenbluth, J. *Int. J. dev. Neurosci.* **6,** 3–24 (1988).
3. Privat, A. C., Jacque, C., Bourre, J. M., Dupouey, P. & Baumann, N. *Neurosci. Lett.* **12,** 107–112 (1979).
4. Roach, A., Takahashi, N., Pravtcheva, D., Ruddle, F. & Hood, L. *Cell* **42,** 149–155 (1985).
5. Molineaux, S. M., Engh, H., deFerra, F., Hudson, L. & Lazzarini, R. A. *Proc. natn. Acad. Sci. U.S.A.* **83,** 7542–7546 (1986).
6. Rosenbluth, J. *J. comp. Neurol.* **194,** 639–648 (1980).
7. Rosenbluth, J. *Brain Res.* **208,** 283–297 (1981).

8. Inoue, Y., Nakamura, R., Mikoshiba, K. & Tsukada, Y. *Brain Res.* **219,** 85–94 (1981).
9. Sharkey, R. G., Beneski, D. & Catterall, W. A. *Biochemistry* **23,** 6078–6086 (1984).
10. Schmidt, J., Rossie, S. & Catterall, W. A. *Proc. natn. Acad. Sci. U.S.A.* **82,** 4847–4851 (1985).
11. Stumer, W., Methfessel, C., Sakman, B., Noda, M. & Numa, S. *Eur. Biophys. J.* **14,** 131–138 (1987).
12. Sontheimer, H., Trotter, J., Schachner, M. & Kettenman, H. *Neuron* **2,** 1135–1145 (1989).
13. Barres, B. A., Chun, L. L. Y. & Corey, D. P. *Neuron* **2,** 1375–1388 (1989).
14. Sheedlo, H. J. & Siegel, G. J. *Brain Res.* **415,** 105–114 (1987).
15. Waxman, S. G., Black, J. A., Duncan, I. D. & Ransom, B. R. *J. Neurocytol.* **19,** 11–27 (1990).
16. Waxman, S. G., Black, J. A., Kocsis, J. D. & Ritchie, J. M. *Proc. natn. Acad. Sci. U.S.A.* **86,** 1406–1410 (1989).
17. Scheinman, R. I. *et al. J. biol. Chem.* **264,** 1060–1066 (1989).
18. Chiu, S. Y. & Schwarz, W. *J. Physiol.* **391,** 631–649 (1987).
19. Caroni, P. & Schwab, M. E. *J. Cell. Biol.* **106,** 1281–1288 (1988).
20. Hodgkin, A. L. *Phil. Trans. R. Soc. Lond.* B **270,** 297–300 (1975).
21. Campagnoni, A. T. *J. Neurochem.* **51,** 1–14 (1988).
22. Lemke, G. *Neuron* **1,** 535–543 (1988).
23. Sorg, B. J., Smith, M. M. & Campagnoni, T. *J. Neurochem.* **49,** 1146–1154 (1987).
24. Frail, D. E. & Braun, P. E. *J. Neurochem.* **45,** 1071–1075 (1985).
25. Wisniewski, H. M., Oppenheimer, D. & McDonald, W. E. *J. Neuropathol. exp. Neurol.* **35,** 327 (1976).
26. Smith, K. J. & McDonald, W. I. *Nature* **286,** 154–155 (1980).
27. Offard, J. & Catterall, W. A. *Neuron* **2,** 1447–1452 (1989).
28. Lidow, M. S., Goldman-Rakic, P. S., Rakic, P. & Gallagher, D. W. *Brain Res.* **459,** 105–119 (1988).
29. Bird, T. D., Farrell, D. F. & Sumo, S. M. *J. Neurochem.* **31,** 387–391 (1978).
30. Mourre, C., Moll, C., Loubet, A. & Lazdunski, M. *Brain Res.* **448,** 128–139 (1988).

ACKNOWLEDGEMENTS. We thank H. D. Shine for electron microscopy of *shiverer* optic nerve. This work was supported by March of Dimes/Birth Defects Foundation, NICHD, Blue Bird Circle Foundation for Pediatric Neurology, and a Pew Biomedical Scholars Award (J.L.N.).

Prevention of HIV-1 IIIB infection in chimpanzees by CD4 immunoadhesin

Rebecca H. R. Ward, Daniel J. Capon*, Catherine M. Jett†, Krishna K. Murthy†, Joyce Mordenti, Catherine Lucas, Steve W. Frie, Alfred M. Prince‡, James D. Green & Jorg W. Eichberg†§

Genentech Inc., 460 Pt San Bruno Boulevard, S. San Francisco, California 94080, USA
* Cell Genesys Inc., 344 Lakeside Drive, Foster City, California 94404, USA
† Southwest Foundation for Biomedical Research, San Antonio, Texas 78284, USA
‡ The Lindsley F. Kimball Research Institute of the NY Blood Center, 310 East 67th Street, New York 10021, USA
§ Present address: Wyeth-Ayerst Research, 145 King of Prussia Road, Philadelphia, Pennsylvania 19087, USA

THE first step in infection by the human immunodeficiency virus (HIV) is the specific binding of gp120, the envelope glycoprotein of HIV, to its cellular receptor, CD4 (see ref. 1 for review). To inhibit this interaction, soluble CD4 analogues that compete for gp120 binding and block HIV infection *in vitro* have been developed[2–8]. To determine whether these analogues can protect an uninfected individual from challenge with HIV, we used the chimpanzee model system of cell-free HIV infection. Chimpanzees are readily infected with the IIIB strain of HIV-1, becoming viraemic within about 4–6 weeks of challenge, although they do not develop the profound CD4$^+$ T-cell depletion and immunodeficiency characteristic of HIV infection in humans[9]. CD4 immunoadhesin (CD4–IgG), a chimaeric molecule consisting of the N-terminal two immunoglobulin-like regions of CD4 joined to the Fc region of human IgG1 (refs 8, 10), was selected as the CD4 analogue for testing because it has a longer half-life than CD4, contributed by the IgG Fc portion of the molecule. In humans, this difference results in a 25-fold increased concentration of CD4–IgG in the blood compared with recombinant CD4 (ref. 11). Here we report that pretreatment with CD4–IgG can prevent the infection of chimpanzees with HIV-1. The need for a preventative agent is particularly acute in perinatal HIV transmission. As recombinant CD4–IgG, like the parent IgG molecule, efficiently crosses the primate placenta[10], it may be possible to set up an immune state in a fetus before HIV transfer occurs, thus preventing infection.

Two chimpanzees were pretreated with CD4–IgG (5 mg kg^{-1} given intravenously (i.v.)) at 8 h and 1 h before challenge, then inoculated with 120 tissue culture infectious doses ($TCID_{50}$s) of HIV-1 IIIB (30 chimp infectious doses). After challenge, the animals received further CD4–IgG treatment for 9 weeks. A control animal was similarly challenged but not treated. This dose of HIV-1 IIIB is expected to result in seroconversion of all untreated animals within 9 weeks (see, for example, ref. 12). The serum concentrations of CD4–IgG were predicted from the known human pharmacokinetics and checked by enzyme-linked immunosorbent assay (ELISA) where indicated (Fig. 1). The serum concentrations of CD4–IgG attained during the first 2 days of treatment were estimated to be 50–200 μg ml^{-1}, and over the next 5 weeks were predicted to be 5–120 μg ml^{-1}; trough concentrations were confirmed by ELISA. When doses were given i.v. (week 6 onwards), the predicted concentrations of 0.5–200 μg ml^{-1} were confirmed by ELISA. Treated animals were also monitored for the development of antibodies to CD4–IgG by indirect ELISA. Chimpanzee 37 transiently showed just detectable antibody levels at weeks 7–13 (not shown). Chimpanzee 43 had no detectable antibody response.

Chimpanzees were monitored for HIV infection by detection of virus and by analysis for seroconversion. Virus was detected by a viral coculture assay, in which p24 production was measured, and by the polymerase chain reaction (PCR). The development of antibodies to HIV proteins was assessed by western blot and ELISA whole-virus based assays. The control animal became infected 3 weeks after challenge, as shown by viral coculture (Table 1), and virus could be detected by PCR at 11 weeks. Antibody to the viral protein p24 became evident in this animal by western blot at week 7 (Fig. 2), and subsequently antibodies to other viral proteins, including gp120, were detected. The animal showed seroconversion to HIV by ELISA at week 7 (Table 1). By contrast, the CD4–IgG-treated animals have not shown any signs of infection, after 47 weeks. A single sample from animal 37 (week 23) was positive in two of three PCR assays using a *gag* primer pair (Table 1), but negative using a pair of *env*-derived primers of identical sensitivity (Table 1 legend). Further samples from the same animal up to week 47 have repeatedly assayed negative by both PCR and viral culture. It thus seems that both treated animals were protected from infection.

Immunization with recombinant gp120 (ref. 13) or successive immunization with a variety of immunogens including the V3 loop of gp120 (ref. 14) can induce protective immunity in chimpanzees against later challenge with HIV-1 IIIB. But passive protection from HIV infection has not been previously shown. Protection of chimpanzees against HIV-1 by pretreatment with a single high dose of purified hyperimmune gammaglobulin (HIVIG) obtained from AIDS patients has been observed (A.M.P. *et al.*, manuscript in preparation). The control animal described here was shared with the HIVIG study. In our study, treatment with CD4–IgG continued for 9 weeks, in contrast to the single dose of HIVIG. Further work is needed to determine the necessary dose and length of treatment with CD4–IgG.

Azidothymidine (AZT), the only drug currently approved for the treatment of AIDS, has not yet been shown to prevent infection by HIV or simian immunodeficiency virus (SIV) in animal models, whether given before[15] or after[16] virus challenge, although it does delay the spread of infection. It is unclear whether AZT can prevent infection after accidental challenge with HIV or maternal–fetal transfer in humans; AZT failures in both forms of challenge are known[17,18]. Clinical trials to address these issues are under way.

Although our results, and those of others (A.M.P. *et al.*, manuscript in preparation), show that it is possible to prevent HIV-1 infection by passive transfer of immunity, it is unclear